ACS APPLIED MATERIALS & INTERFACES

Research Article

www.acsami.org

Nitrogen-Doped Carbon-Wrapped Porous Single-Crystalline CoO Nanocubes for High-Performance Lithium Storage

Kongwei Xie, Ping Wu,* Yunyun Zhou, Ya Ye, Hui Wang, Yawen Tang, Yiming Zhou,* and Tianhong Lu

Jiangsu Key Laboratory of New Power Batteries, Jiangsu Collaborative Innovation Center of Biomedical Functional Materials, School of Chemistry and Materials Science, Nanjing Normal University, Nanjing 210023, P. R. China

Supporting Information

ABSTRACT: Herein, we have designed and synthesized a novel type of nitrogen-doped carbon-supported CoO nanohybrids, i.e., nitrogen-doped carbon-wrapped porous single-crystalline CoO nanocubes (CoO@N−C nanocubes), by using Co_3O_4 nanocubes as precursors. Owing to its unique structural features, the as-synthesized CoO@N−C nanocubes demonstrate markedly enhanced anodic performance in terms of reversible capacity, cycling stability, and rate capability, facilitating its application as a high-capacity, long-life, and high-rate anode for advanced lithium-ion batteries.

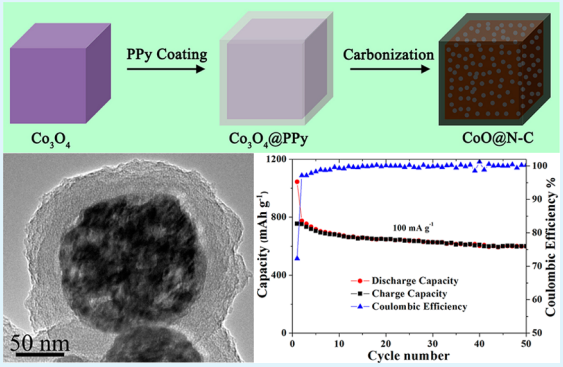

KEYWORDS: *lithium-ion batteries, anodes, CoO, nitrogen-doped carbon, porous single-crystalline nanocubes*

1. INTRODUCTION

Since the pioneering work of Tarascon et al. in 2000,[1] much research interest has concentrated on a new anodic category for lithium-ion batteries (LIBs), i.e., 3d transition-metal oxides (M_xO_y, M = Fe, Co, Ni, and Cu).[2−7] Typically, cobalt monoxide (CoO) has been regarded as an ideal anodic candidate to replace commercial graphitic materials owing to its high theoretical capacity (715 mA h g^{-1}).[8−11] However, CoO anodes still suffer from low intrinsic electrical conductivity and poor structural stability during lithium insertion/extraction, which leads to low rate capability and poor cycling stability and thus hinders its practical application in advanced LIBs.

Up to now, extensive work has proceeded to address these issues via the microscopic structural design of CoO anodes.[8−19] Among them, nanostructuring and hybridizing anodic systems with carbon (C) matrixes have proven to be an effective design strategy to improve their lithium-storage capabilities.[12−23] For example, amorphous carbon,[12−14] graphitic carbon,[15] carbon nanotubes (CNTs),[16] and graphene[17−19] supported nanostructured CoO anodes are able to exhibit improved strain accommodation and charge-transport capabilities and thus enhanced cycling stability and rate capability. Recently, it has been reported that nitrogen (N) doping can improve the electrical conductivity and interfacial stability and promote the reaction kinetics of C-based electrodes in energy storage and conversion devices including LIBs,[24−28] fuel cells,[29] and supercapacitors.[30−33] For example, N-doped carbon has been adopted as an efficient conducting and buffering matrix for Fe_3O_4,[26] Sn,[27] and $Li_4Ti_5O_{12}$[28] anodes in LIBs owing to the enhanced lithium-storage reaction kinetics. Therefore, N-doped C-supported CoO nanohybrids are expected to demonstrate further enhanced anodic performance in LIBs and meet the commercial requirements of advanced anodes with high capacity, long life, and high rate.

Herein, we have designed and synthesized a novel type of N-doped C-supported CoO nanohybrids, i.e., N-doped C-wrapped porous single-crystalline CoO nanocubes (CoO@N−C nanocubes), by using Co_3O_4 nanocubes as precursors. When examined as a potential anode for LIBs, the as-synthesized CoO@N−C nanocubes demonstrate superior lithium-storage capabilities in terms of reversible capacity, cycling stability, and rate capability.

2. EXPERIMENTAL SECTION

Synthesis of CoO@N−C Nanocubes. The precursor, i.e., Co_3O_4 nanocubes, was prepared via a hydrothermal method. Briefly, 1 g of poly(vinylpyrrolidone) was dissolved in 20 mL 7 M ammonia to form a clear solution, and then 5 mL of 1 M cobalt acetate was added dropwise. After stirring for 10 min, the mixture was sealed in a Teflon-lined stainless steel autoclave and maintained at 160 °C for 16 h. Then, the resulting black product was washed with distilled water and ethanol and then dried at 80 °C in air. The as-prepared Co_3O_4 nanocubes were wrapped by polypyrrole (PPy) through a chemical oxidative polymerization of pyrrole monomers by using $(NH_4)_2S_2O_8$ as an oxidant.[7] Finally, the Co_3O_4@PPy nanocubes were kept in a tube furnace at 500 °C for 3 h under N_2 at a ramping rate of 2 °C min^{-1}, resulting in CoO@N−C nanocubes.

Characterization. The morphology, structure, and composition of the products were characterized by scanning electron microscopy

Received: April 14, 2014
Accepted: June 17, 2014
Published: June 17, 2014

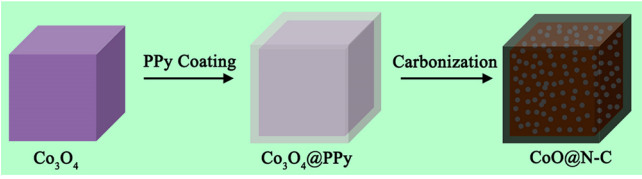

Figure 1. Schematic illustration of the fabrication for CoO@N−C nanocubes.

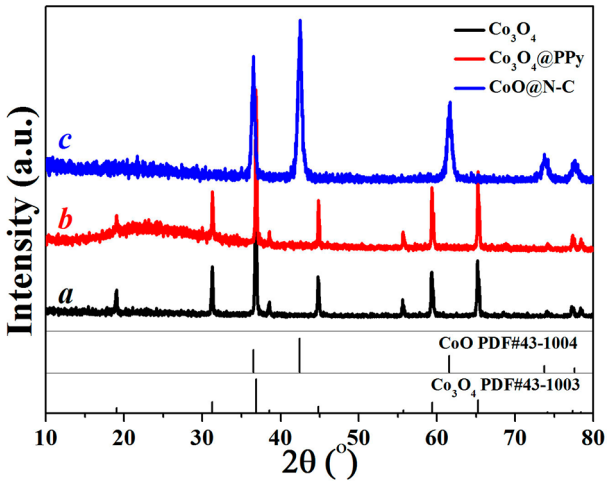

Figure 2. XRD patterns of Co_3O_4 (curve a), Co_3O_4@PPy (curve b), and CoO@N−C (curve c) nanocubes.

(SEM; JEOL JSM-7600F), transmission electron microscopy (TEM; Hitachi H-7650, 120 kV), and high-resolution transmission electron microscopy (HRTEM; JEOL JEM-2010F, 200 kV) coupled with energy-dispersive X-ray spectrometry (EDX; Thermo Fisher Scientific). Powder X-ray diffraction (XRD) measurements were performed with a model D/max-rC diffractometer using Cu Kα radiation (λ = 0.15406 nm) and operating at 45 kV and 100 mA. Thermogravimetric analysis (TGA) was carried out on a Netzsch STA 449C thermal analyzer at a heating rate of 10 °C min^{-1} in air. X-ray photoelectron spectroscopy (XPS) analysis was performed on a Thermo VG Scientific ESCALAB 250 spectrometer with a monochromatic Al Kα X-ray source (1486.6 eV photons).

Electrochemical Measurements of CoO@N−C Nanocubes. Electrochemical tests were carried out by 2025-type coin cells, which were assembled in an Ar-filled glovebox (IL-2GB, Innovative Technology). The electrodes were made as follows: 70 wt % CoO@N−C nanocubes, 15 wt % Super P, and 15 wt % poly(vinylidene fluoride) in *N*-methyl-2-pyrrolidene were mixed, and then the slurry was coated on the surface of copper foams and dried under vacuum at 120 °C for 12 h. An N-doped carbon matrix in CoO@N−C nanocubes was considered as part of the active material during calculation of the specific capacity of a nanohybrid anode, and the loading density of the active material on copper foam current collectors was ca. 1.5 mg cm^{-2}. The counter electrode was lithium foil, and the electrolyte solution was 1 M $LiPF_6$ in ethylene carbonate and dimethyl carbonate (1:1 by volume). Finally, the cells were aged for 12 h before measurements. A galvanostatic cycling test of the assembled cells was examined on a Land CT2001A system in the potential range of 0.01−3 V. Cyclic voltammtery (CV) measurements were recorded on a CHI 660C electrochemical workstation in the potential range of 0.0−3 V at a scan rate of 0.1 mV s^{-1}. The voltages mentioned herein were referred to a Li^+/Li redox couple. All of the electrochemical measurements were conducted at 20 °C.

3. RESULTS AND DISCUSSION

Figure 1 depicts the schematic diagram for the formation of CoO@N−C nanocubes. As observed, the Co_3O_4 nanocubes are prepared via a facile hydrothermal method and act as precursors in this synthetic methodology. Concretely, Co_3O_4 nanocubes have been transformed into Co_3O_4@PPy and CoO@N−C nanocubes after subsequent PPy coating and carbonization processes. Figure 2 shows the corresponding XRD patterns of the Co_3O_4, Co_3O_4@PPy, and CoO@N−C nanocubes. The observed crystalline phase has transformed from cubic Co_3O_4 (curves a

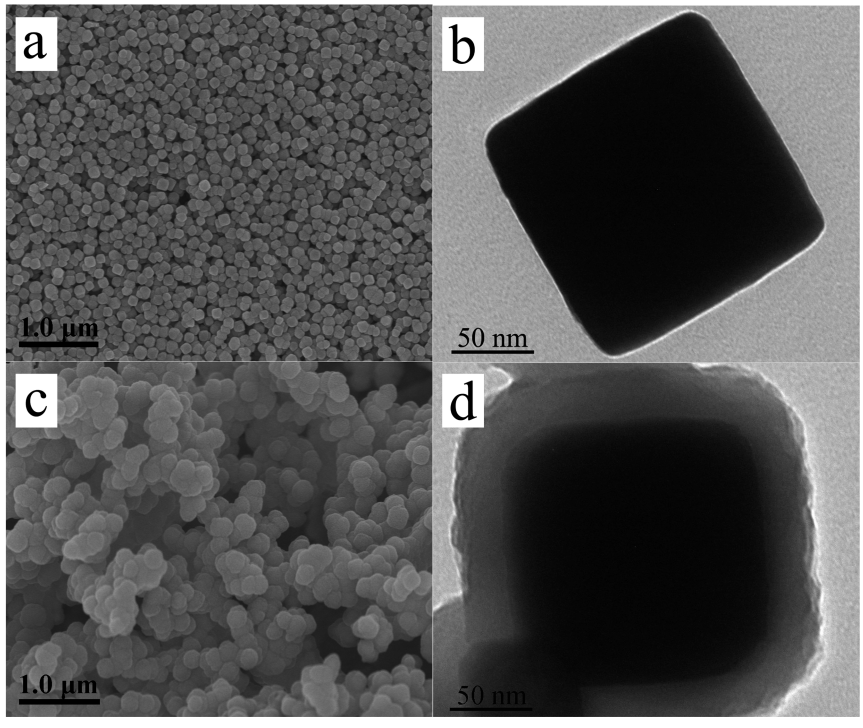

Figure 3. SEM and TEM images of Co_3O_4 (a and b) and Co_3O_4@PPy (c and d) nanocubes.

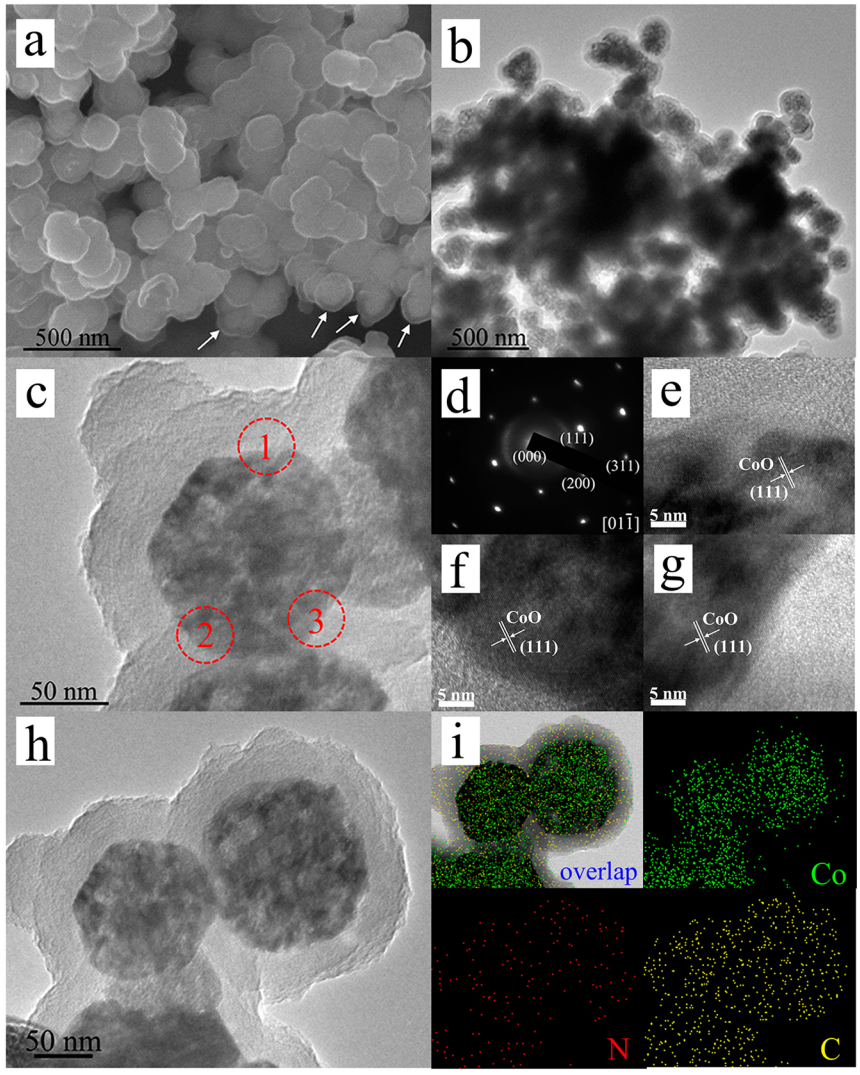

Figure 4. Morphological, structural, and compositional characterizations of CoO@N−C nanocubes: (a) SEM image; (b) TEM image; (c and d) TEM image and its SAED pattern; (e−g) HRTEM images of regions 1−3 shown in part c, respectively; (h and i) TEM−EDX elemental mappings of Co (green), N (red), and C (yellow) and their overlap.

and b; PDF card 43-1003) to cubic CoO (curve c; PDF card 43-1004), whereas the PPy- and N-doped carbon layers are not well crystallized.

The morphological and structural characterizations of Co_3O_4 and Co_3O_4@PPy nanocubes were examined by SEM and TEM (Figure 3). The Co_3O_4 products exhibit typical cubelike morphology with a size length of ca. 150 nm and a smooth surface (Figure 3a,b). Subsequently, the Co_3O_4 nanocubes are fully wrapped by a PPy layer after chemical oxidative polymerization of pyrrole (Figure 3c,d). As observed, the cubic morphology is well retained in Co_3O_4@PPy nanocubes, and the average thickness of the uniform PPy layer in the core−shell nanocubes is ca. 30 nm.

Furthermore, the as-prepared Co_3O_4@PPy nanocubes could be converted into CoO@N−C nanocubes through a controlled annealing process at a relatively lower temperature (500 °C). During the thermal treatment process, the PPy precursor has been carbonized into a N−C layer,[25] and the N−C hollow nanocube could simultaneously serve as a novel nanoreactor for the reduction of Co_3O_4 to CoO. Figure 4 shows the morphological, structural, and compositional characterizations of the CoO@N−C nanocubes. As observed, the cubic morphology and core−shell structure are both well preserved in the product (Figure 4a,b). The TEM images clearly reveal that the CoO core exists in the form of a porous nanocube, which is fully encapsulated in a N−C layer with a thickness of ca. 30 nm (Figure 4b,c). Figure 4d displays its selected-area electron diffraction (SAED) pattern recorded along the [01−1] zone axis. The observed diffraction spots from the SAED pattern can all be indexed to CoO with cubic symmetry, suggesting the single-crystalline nature of the CoO core. Parts e−g of Figure 4 show the HRTEM images of three representative areas taken from regions 1−3 shown in Figure 4c. As can be seen, the whole CoO core grows along the same direction, further confirming the single crystallinity of the CoO nanocube. Parts h and i of Figure 4 show a typical TEM image of CoO@N−C nanocubes along with its corresponding elemental mappings of Co (green), N (red), and C (yellow) and their overlap. As can be seen, the Co element is concentrated in the core region, whereas N and C signals are uniformly distributed in the selected area, confirming the formation of a core−shell structure and homogeneous N doping in carbon shells.

Moreover, the N content in PPy-derived carbon was examined by XPS. As observed in Figure 5, the molar ratio of N/C in a N−C

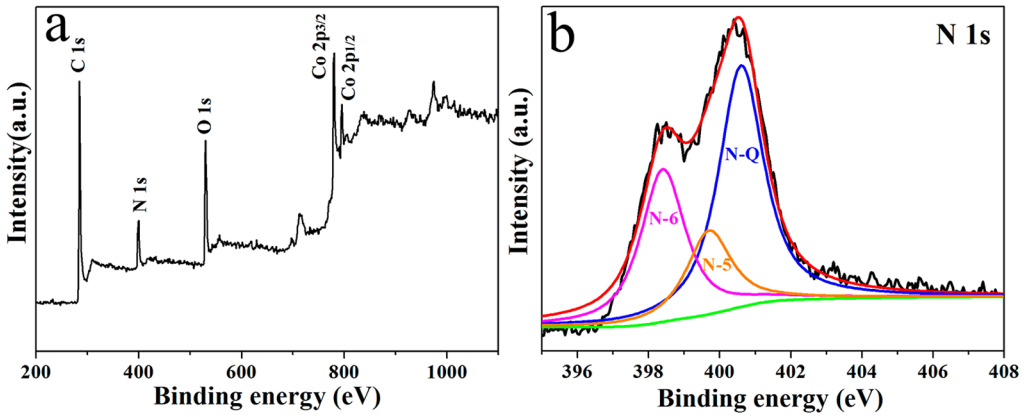

Figure 5. XPS spectra of CoO@N−C nanocubes: (a) survey spectrum; (b) N 1s spectrum.

layer is determined to be ca. 0.18, which is lower than the value of the PPy unit (−C_4NH_2−, 0.25) because of its partial carbonization.[31] Additionally, the N 1s spectrum can be deconvoluted into three components, i.e., pyridinic N (N-6), pyrrolic N (N-5), and quaternary N (N-Q), which are located at ca. 398.4, 399.7, and 400.6 eV, respectively.[31,32] Carbonization of the PPy layer leads to the appearance of N-6 and N-Q peaks with much stronger intensities compared with that of the N-5 peak, which is beneficial for the enhanced reaction kinetics toward lithium storage.[24−27] TGA was further performed to quantitatively determine the N−C content presented in the CoO@N−C nanocubes (Figure S1 in the Supporting Information, SI). Removal of the N−C layer leads to a weight decrease and oxidation of the CoO component gives rise to a weight increase of the product. The observed weight loss between 200 and 737 °C could be mainly attributed to combustion of the N−C shell, whereas the subsequent weight gain is probably related to oxidation of CoO to Co_3O_4. Thus, the N−C content in CoO@N−C nanocubes can be determined to be ca. 21.5 wt %.

Motivated by its unique microscopic structural features, we performed the anodic performance of CoO@N−C nanocubes for LIBs in comparison with bare Co_3O_4 nanocubes. Figure 6 shows the first three CV curves of CoO@N−C nanocubes in the potential range of 0.0−3.0 V at a scan rate of 0.1 mV s^{-1}. The profiles of these curves are in good accordance with the lithium-storage mechanism for CoO-based anodes as described previously:

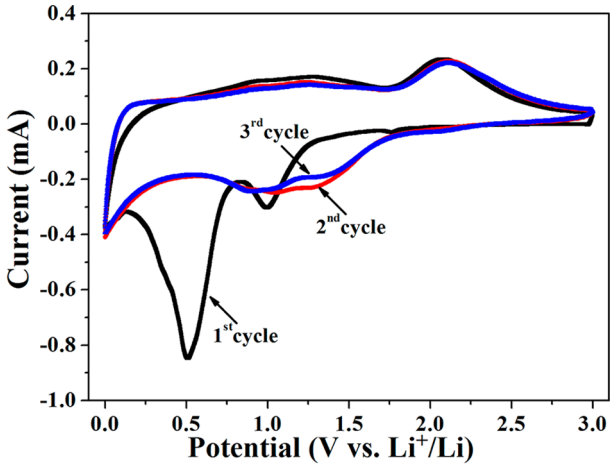

Figure 6. First three CV curves of CoO@N−C nanocubes in the potential range of 0.0−3 V at a scan rate of 0.1 mV s^{-1}.

$CoO + 2Li^+ + 2e^- \leftrightarrow Co + Li_2O$.[1] In the first cycle, the cathodic peaks at ca. 1.0 V can be assigned to the lithium insertion into a CoO crystal and partial reduction of CoO, whereas the subsequent peak at ca. 0.5 V corresponds to destruction of the crystal structure, reduction of CoO to Co, and also formation of the solid electrolyte interface (SEI) layer.[19,34] The cathodic peaks shift to higher voltages at ca. 0.9 and 1.3 V in subsequent cycles, which is probably because of the decreased surface energy of the CoO anode after the initial lithiation/delithiation process.[15,18,35] For the anodic processes, the peak at 2.1 V can be attributed to oxidation from Co^0 to Co^{2+}.[35]

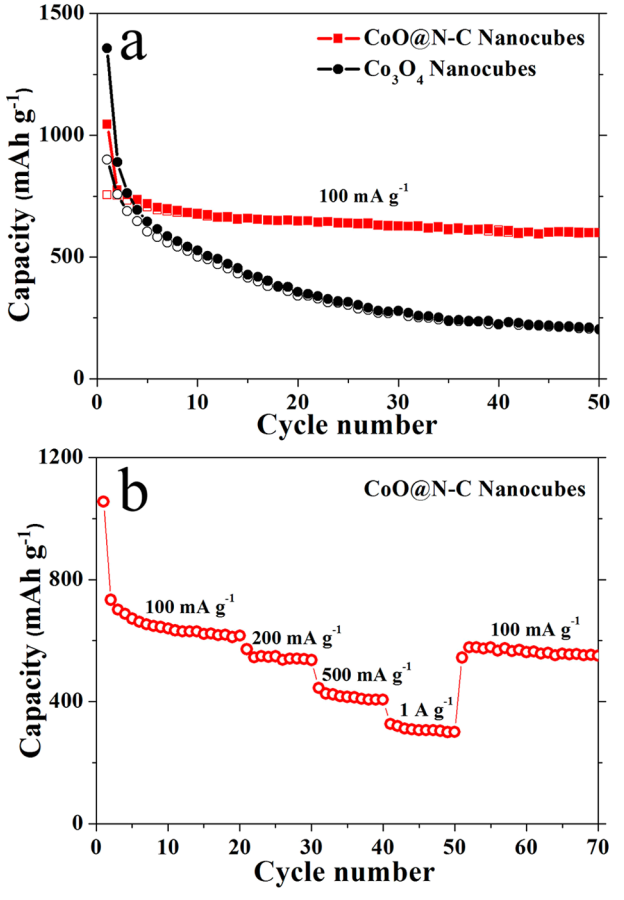

Figure 7. Lithium-storage performance of CoO@N−C and bare Co_3O_4 nanocubes: (a) cycling performance; (b) rate capability.

dx.doi.org/10.1021/am502214k | ACS Appl. Mater. Interfaces 2014, 6, 10602−10607

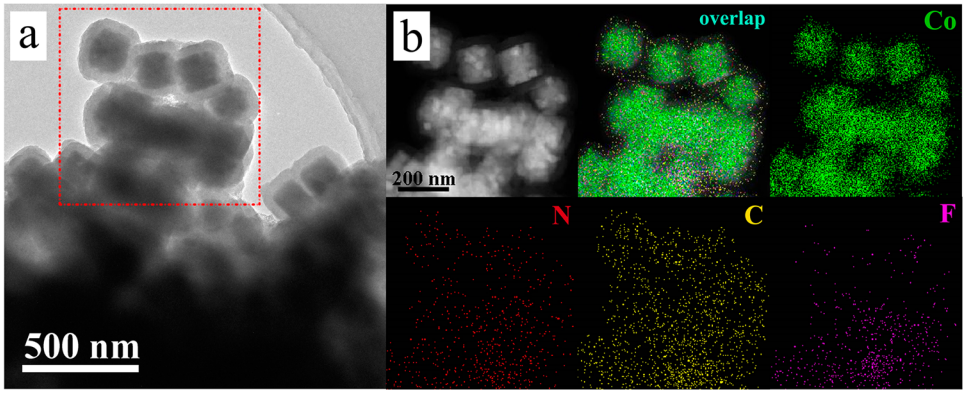

Figure 8. TEM image (a) along with the corresponding EDX elemental mappings (b) of CoO@N−C nanocubes in a fully delithiated state (3 V vs Li^+/Li) after 50 cycles.

Figure 7a shows the cycling stability for CoO@N−C and bare Co_3O_4 nanocubes in the potential range of 0.01−3 V at a current density of 100 mA g^{-1}. As observed, the discharge and charge capacities of CoO@N−C nanocubes in the first cycle are 1044.0 and 754.5 mA h g^{-1}, respectively, corresponding to a Coulombic efficiency of 72.3% (Figure S2 in the SI). The initial capacity loss (289.5 mA h g^{-1}) could be mainly attributed to the irreversible formation of the SEI layer. Despite this, the CoO@N−C nanocubes demonstrate markedly enhanced cycling stability than bare Co_3O_4 nanocubes, and the Coulombic efficiencies of CoO@N−C nanocubes remain steadily at more than 97% after the first cycle (Figure S3 in the SI). After 50 cycles, the CoO@N−C nanocubes are able to deliver a high discharge capacity of 598.3 mA h g^{-1}, which is much higher than the theoretical capacity of graphite (372 mA h g^{-1}) and that of bare Co_3O_4 nanocubes (203.7 mA h g^{-1}). The high reversible capacity and excellent capacity retention of CoO@N−C nanocubes facilitate its application as a high-capacity and long-life anode for advanced LIBs. Figure 7b displays the rate capability of CoO@N−C nanocubes at various current densities from 100 to 200, 500, and 1000 mA g^{-1} and finally back to 100 mA g^{-1}. The discharge capacities vary along with charging/discharging rates, and the average values decrease from 646.0 to 545.4, 416.9, and 309.0 mA h g^{-1} and finally recover to 562.4 mA h g^{-1}. Additionally, the profiles of the corresponding discharge/charge curves are in good agreement with the conversion-type lithium-storage mechanism of CoO-based anodes (Figure S4 in the SI). These results demonstrate the high rate capability of CoO@N−C nanocubes, making it an ideal anode candidate for high-power LIBs.

The improved lithium-storage capabilities, especially cycling stability, could be attributed to the enhanced structural stability during lithium insertion and extraction, which can be confirmed by their microstructural characterizations after cycling. Figure 8 displays the TEM−EDX elemental mappings of CoO@N−C nanocubes in a fully delithiated state (3 V vs Li^+/Li) after 50 cycles. As observed from the TEM images, the cubic morphology and core−shell structure are still well retained in the delithiated product. The Co, N, and C signals from EDX elemental mappings are uniformly distributed in the core area and entire product, respectively, and are in good agreement with the TEM images. Additionally, the F signal might originate from the SEI layer on the surface of the CoO@N−C anode.[36] The TEM and elemental mapping characterizations indicate that anodic agglomeration, pulverization, and detachment could be effectively suppressed during repeated lithium insertion/extraction. Thus, the CoO@N−C nanocubes manifest enhanced structural stability upon cycling and markedly improved lithium-storage capabilities.

4. CONCLUSION

In summary, a novel type of N-doped C-supported CoO nanohybrids, i.e., N-doped C-wrapped porous single-crystalline CoO nanocubes (CoO@N−C nanocubes), has been designed and synthesized by using Co_3O_4 nanocubes as precursors. When tested as an anode material for LIBs, the CoO@N−C nanocubes display high capacity, remarkable cycling stability, and high rate capability. For example, a high reversible capacity of 598.3 mA h g^{-1} can be retained after 50 cycles at a current density of 100 mA g^{-1}. The superior lithium-storage capability of CoO@N−C nanocubes makes it an ideal anode candidate for high-energy, long-life, and high-power LIBs.

■ ASSOCIATED CONTENT

Ⓢ Supporting Information

TGA curves and discharge and charge curves of CoO@N−C nanocubes and Coulombic efficiencies for CoO@N−C and bare Co_3O_4 nanocubes. This material is available free of charge via the Internet at http://pubs.acs.org.

■ AUTHOR INFORMATION

Corresponding Authors

*E-mail: zjuwuping@njnu.edu.cn.
*E-mail: zhouyiming@njnu.edu.cn.

Notes

The authors declare no competing financial interest.

■ ACKNOWLEDGMENTS

We appreciate financial support from the Natural Science Foundation of Jiangsu Province (Grant BK20130900), Natural Science Foundation of Jiangsu Higher Education Institutions of China (Grant 13KJB150026), Industry−Academia Cooperation Innovation Fund Project of Jiangsu Province (Grants BY2013001-01 and BY2012001), Priming Scientific Research Foundation for Advanced Talents in Nanjing Normal University (Grant 2013103XGQ0008), and a project funded by the Priority Academic Program Development of Jiangsu Higher Education Institutions. Dedicated to Professor Xinquan Xin on the occasion of his 80th birthday.

REFERENCES

(1) Poizot, P.; Laruelle, S.; Dupont, L.; Tarascon, J. M. Nano-Sized Transition-Metal Oxides as Negative-Electrode Materials for Lithium-Ion Batteries. *Nature* **2000**, *407*, 496−499.

(2) Ji, L.; Toprakci, Q.; Alcoutlabi, M.; Yao, Y.; Li, Y.; Zhang, S.; Guo, B.; Lin, Z.; Zhang, X. α-Fe_2O_3 Nanoparticle-Loaded Carbon Nanofibers as Stable and High-Capacity Anodes for Rechargeable Lithium-Ion Batteries. *ACS Appl. Mater. Interfaces* **2012**, *4*, 2672−2679.

(3) Lang, L.; Xu, Z. In Situ Synthesis of Porous Fe_3O_4/C Microbelts and Their Enhanced Electrochemical Performance for Lithium-ion Batteries. *ACS Appl. Mater. Interfaces* **2013**, *5*, 1698−1703.

(4) Liu, Y.; Mi, C.; Su, L.; Zhang, X. Hydrothermal Synthesis of Co_3O_4 Microspheres as Anode Material for Lithium-Ion Batteries. *Electrochim. Acta* **2008**, *53*, 2507−2513.

(5) Tao, L.; Zai, J.; Wang, K.; Zhang, H.; Xu, M.; Shen, J.; Su, Y.; Qian, X. Co_3O_4 Nanorods/Graphene Nanosheets Nanocomposites for Lithium Ion Batteries with Improved Reversible Capacity and Cycle Stability. *J. Power Sources* **2012**, *202*, 230−235.

(6) Zai, J.; Yu, C.; Tao, L.; Xu, M.; Xiao, Y.; Li, B.; Han, Q.; Wang, K.; Qian, X. Synthesis of Ni-Doped NiO/RGONS Nanocomposites with Enhanced Rate Capabilities as Anode Materials for Li Ion Batteries. *CrystEngComm* **2013**, *15*, 6663−6671.

(7) Yin, Z.; Ding, Y.; Zheng, Q.; Guan, L. CuO/Polypyrrole Core−Shell Nanocomposites as Anode Materials for Lithium-Ion Batteries. *Electrochem. Commun.* **2012**, *20*, 40−43.

(8) Guan, H.; Wang, X.; Li, H.; Zhi, C.; Zhai, T.; Bando, Y.; Golberg, D. CoO Octahedral Nanocages for High-Performance Lithium Ion Batteries. *Chem. Commun.* **2012**, *48*, 4878−4880.

(9) Sun, Y.; Hu, X.; Luo, W.; Huang, Y. Self-Assembled Mesoporous CoO Nanodisks as a Long-Life Anode Material for Lithium-Ion Batteries. *J. Mater. Chem.* **2012**, *22*, 13826−13831.

(10) Qi, Y.; Du, N.; Zhang, H.; Fan, X.; Yang, Y.; Yang, D. CoO/$NiSi_x$ Core−Shell Nanowire Arrays as Lithium-Ion Anodes with High Rate Capabilities. *Nanoscale* **2012**, *4*, 991−996.

(11) Zheng, X.; Shen, G.; Li, Y.; Duan, H.; Yang, X.; Huang, S.; Wang, H.; Wang, C.; Deng, Z.; Su, B. L. Self-Templated Synthesis of Microporous CoO Nanoparticles with Highly Enhanced Performance for Both Photocatalysis and Lithium-Ion Batteries. *J. Mater. Chem. A* **2013**, *1*, 1394−1400.

(12) Yuan, W.; Zhang, J.; Xie, D.; Dong, Z.; Su, Q.; Du, G. Porous CoO/C Polyhedra as Anode Material for Li-Ion Batteries. *Electrochim. Acta* **2013**, *108*, 506−511.

(13) Xiong, S.; Chen, J. S.; Lou, X. W.; Zeng, H. C. Mesoporous Co_3O_4 and CoO@C Topotactically Transformed from Chrysanthemum-Like $Co(CO_3)_{0.5}(OH)\cdot 0.11H_2O$ and Their Lithium-Storage Properties. *Adv. Funct. Mater.* **2012**, *22*, 861−871.

(14) Liu, J.; Zhou, Y.; Liu, C.; Wang, J.; Pan, Y.; Xue, D. Self-Assembled Porous Hierarchical-Like CoO@C Microsheets Transformed from Inorganic−Organic Precursors and Their Lithium-Ion Battery Application. *CrystEngComm* **2012**, *14*, 2669−2674.

(15) Li, F.; Zou, Q. Q.; Xia, Y. Y. CoO-Loaded Graphitable Carbon Hollow Spheres as Anode Materials for Lithium-Ion Battery. *J. Power Sources* **2008**, *177*, 546−552.

(16) Kim, J. C.; Hwang, I. S.; Seo, S. D.; Kim, D. W. Nanocomposite Li-Ion Battery Anodes Consisting of Multiwalled Carbon Nanotubes that Anchor CoO Nanoparticles. *Mater. Lett.* **2013**, *104*, 13−16.

(17) Peng, C.; Chen, B.; Qin, Y.; Yang, S.; Li, C.; Zuo, Y.; Liu, S.; Yang, J. Facile Ultrasonic Synthesis of CoO Quantum Dot/Graphene Nanosheet Composites with High Lithium Storage Capacity. *ACS Nano* **2012**, *6*, 1074−1081.

(18) Sun, Y.; Hu, X.; Luo, W.; Huang, Y. Ultrathin CoO/Graphene Hybrid Nanosheets: a Highly Stable Anode Material for Lithium-Ion Batteries. *J. Phys. Chem. C* **2012**, *116*, 20794−20799.

(19) Qi, Y.; Zhang, H.; Du, N.; Yang, D. Highly Loaded CoO/Graphene Nanocomposites as Lithium-Ion Anodes with Superior Reversible Capacity. *J. Mater. Chem. A* **2013**, *1*, 2337−2342.

(20) Han, Q.; Zai, J.; Xiao, Y.; Li, B.; Xu, M.; Qian, X. Direct Growth of SnO_2 Nanorods on Graphene as High Capacity Anode Materials for Lithium Ion Batteries. *RSC Adv.* **2013**, *3*, 20573−20578.

(21) Xiao, Y.; Zai, J.; Tao, L.; Li, B.; Han, Q.; Yu, C.; Qian, X. $MnFe_2O_4$−Graphene Nanocomposites with Enhanced Performances as Anode Materials for Li-Ion Batteries. *Phys. Chem. Chem. Phys.* **2013**, *15*, 3939−3945.

(22) Li, B.; Zai, J.; Xiao, Y.; Han, Q.; Qian, X. SnO_2/C Composites Fabricated by a Biotemplating Method from Cotton and Their Electrochemical Performances. *CrystEngComm* **2014**, *16*, 3318−3322.

(23) Xiao, Y.; Zai, J.; Li, X.; Gong, Y.; Li, B.; Han, Q.; Qian, X. Polydopamine Functionalized Graphene/$NiFe_2O_4$ Nanocomposite with Improving Li Storage Performances. *Nano Energy* **2014**, *6*, 51−58.

(24) Qie, L.; Chen, W.; Wang, Z.; Shao, Q.; Li, X.; Yuan, L.; Hu, X.; Zhang, W.; Huang, Y. Nitrogen-Doped Porous Carbon Nanofiber Webs as Anodes for Lithium Ion Batteries with a Superhigh Capacity and Rate Capability. *Adv. Mater.* **2012**, *24*, 2047−2050.

(25) Wang, Z.; Xiong, X.; Qie, L.; Huang, Y. High-Performance Lithium Storage in Nitrogen-Enriched Carbon Nanofiber Webs Derived from Polypyrrole. *Electrochim. Acta* **2013**, *106*, 320−326.

(26) Ming, H.; Ming, J.; Li, X.; Zhou, Q.; Jin, L.; Fu, Y.; Adkins, J.; Kang, Z.; Zheng, J. Synthesis of N-Doped Carbon Coated Metal Oxide Nanoparticles for Enhanced Li-Ion Storage Ability. *RSC Adv.* **2013**, *3*, 15613−15617.

(27) Chen, J.; Yang, L.; Fang, S.; Zhang, Z.; Deb, A.; Hirano, S. Sn-Contained N-Rich Carbon Nanowires for High-Capacity and Long-Life Lithium Storage. *Electrochim. Acta* **2014**, *127*, 390−396.

(28) Ding, Z.; Zhao, L.; Suo, L.; Jiao, Y.; Meng, S.; Hu, Y.; Wang, Z.; Chen, L. Towards Understanding the Effects of Carbon and Nitrogen-Doped Carbon Coating on the Electrochemical Performance of $Li_4Ti_5O_{12}$ in Lithium Ion Batteries: a Combined Experimental and Theoretical Study. *Phys. Chem. Chem. Phys.* **2011**, *13*, 15127−15133.

(29) Chen, S.; Bi, J.; Zhao, Y.; Yang, L.; Zhang, C.; Ma, Y.; Wu, Q.; Wang, X.; Hu, Z. Nitrogen-Doped Carbon Nanocages as Efficient Metal-Free Electrocatalysts for Oxygen Reduction Reaction. *Adv. Mater.* **2012**, *24*, 5593−5597.

(30) Xu, B.; Zheng, D.; Jia, M.; Cao, G.; Yang, Y. Nitrogen-Doped Porous Carbon Simply Prepared by Pyrolyzing a Nitrogen-Containing Organic Salt for Supercapacitors. *Electrochim. Acta* **2013**, *98*, 176−182.

(31) Su, F.; Poh, C. K.; Chen, J. S.; Xu, G.; Wang, D.; Li, Q.; Lin, J.; Lou, X. Nitrogen-Containing Microporous Carbon Nanospheres with Improved Capacitive Properties. *Energy Environ. Sci.* **2011**, *4*, 717−724.

(32) Chen, L. F.; Zhang, X. D.; Liang, H. W.; Kong, M.; Guan, Q. F.; Chen, P.; Wu, Z. Y.; Yu, S. H. Synthesis of Nitrogen-Doped Porous Carbon Nanofibers as an Efficient Electrode Material for Supercapacitors. *ACS Nano* **2012**, *6*, 7092−7102.

(33) Zhang, D.; Zheng, L.; Ma, Y.; Lei, L.; Li, Q.; Luo, H.; Feng, H.; Hao, Y. Synthesis of Nitrogen- and Sulfur-Codoped 3D Cubic-Ordered Mesoporous Carbon with Superior Performance in Supercapacitors. *ACS Appl. Mater. Interfaces* **2014**, *6*, 2657−2665.

(34) Reddy, M. V.; Prithvi, G.; Loh, K.; Chowdari, B. V. R. Li Storage and Impedance Spectroscopy Studies on Co_3O_4, CoO, and CoN for Li-Ion Batteries. *ACS Appl. Mater. Interfaces* **2014**, *6*, 680−690.

(35) Zhang, M.; Jia, M.; Jin, Y.; Shi, X. Synthesis and Electrochemical Performance of CoO/Graphene Nanocomposite as Anode for Lithium Ion Batteries. *Appl. Surf. Sci.* **2012**, *263*, 573−578.

(36) Chen, L.; Wu, P.; Wang, H.; Ye, Y.; Xu, B.; Cao, G.; Zhou, Y.; Lu, T.; Yang, Y. Highly Loaded SnO_2/Mesoporous Carbon Nanohybrid with Well-Improved Lithium Storage Capability. *J. Power Sources* **2014**, *247*, 178−183.